Kinetic Event-Chain Algorithm for Active Matter: Supplemental Material

Nico Schaffrath, Thevashangar Sathiyanesan, Tobias A. Kampmann, and Jan Kierfeld*
Physics Department, TU Dortmund University, 44221 Dortmund, Germany

CONTENTS

I. DETAILS OF THE KEC ALGORITHM

A. The algorithm

The kEC algorithm is based on the ECMC algorithm for hard disks. Through factorization of the Metropolis filter each interaction can be handled entirely independently. Roughly speaking, each interaction gets a budget of a Boltzmann distributed energy that it uses to overcome energy barriers. The distance until the budget is empty sets the *rejection distance* $d_{\rm rej}$ for each interaction. After all interactions are evaluated, the shortest distance $\min_{\rm interactions}(d_{\rm rej})$ is moved and the EC is lifted to the corresponding interaction partner, while the EC move direction $\boldsymbol{e}_{\rm EC}$ remains. An EC is terminated when the sum of all displacements reach a pre-set length $\ell_{\rm EC}$. In the presence of active forces, the corresponding linear one-particle potentials can also trigger rejection, which results in lifting of the EC direction to its reflection with respect to the equipotential surface ($\boldsymbol{e}'_{\rm EC} = \boldsymbol{e}_{\rm EC} - 2\mathbf{e}_i(\mathbf{e}_i \cdot \boldsymbol{e}_{\rm EC})$), while the moving particle remains the same.

In a more structured way, an EC for active disks of diameters σ_i is constructed as follows:

- Choose random particle i and direction $\boldsymbol{e}_{\rm EC}$ ($|\boldsymbol{e}_{\rm EC}| = 1$) and determine $d_{\rm rej}$, next active particle $i_{\rm next}$ and eventually new EC-direction $\boldsymbol{e}_{\rm EC,next}$
- Initial values
  $d_{\rm rej} = \ell_{\rm EC}$
  $i_{\rm next} = i$
  $\boldsymbol{e}_{\rm EC,next} = \boldsymbol{e}_{\rm EC}$
- Hard Disks:
  for each particle $j \neq i$
  $\mathbf{R} = \mathbf{r}_j - \mathbf{r}_i$
  $\sigma_{ij} = 0.5(\sigma_i + \sigma_j)$
  $x = \mathbf{R} \cdot \boldsymbol{e}_{\rm EC}$
  if $x > 0$ (particles approach each other)
  $y = \sigma_{ij}^2 - \mathbf{R}^2 + x^2$
  if $y > 0$ (particles can hit each other)
  $d_{{\rm rej},ij} = x - \sqrt{y}$
  if $d_{{\rm rej},ij} < d_{\rm rej}$ (event before current one)
  $d_{\rm rej} = d_{{\rm rej},ij}$
  $i_{\rm next} = j$
  $\boldsymbol{e}_{\rm EC,next} = \boldsymbol{e}_{\rm EC}$
- Active Force (**if** $F_{0,i} \neq 0$):
  $x = F_{0,i}(\mathbf{e}_i \cdot \boldsymbol{e}_{\rm EC})$
  if $x < 0$ (particle moves against the force)
  $y = {\rm rand}[0 \ldots 1]$
  $d_{\rm rej,active} = \ln y / \beta x$
  if $d_{\rm rej,active} < d_{\rm rej}$ (event before current one)
  $d_{\rm rej} = d_{\rm rej,active}$
  $i_{\rm next} = i$
  $\boldsymbol{e}_{\rm EC,next} = \boldsymbol{e}_{\rm EC} - 2\mathbf{e}_i(\mathbf{e}_i \cdot \boldsymbol{e}_{\rm EC})$

* jan.kierfeld@tu-dortmund.de

- Execute:

  $\mathbf{r}_i \mathrel{+}= d_{\rm rej}\boldsymbol{e}_{\rm EC}$

  $d_i \mathrel{+}= d_{\rm rej}$

  $\ell_{\rm EC} = \ell_{\rm EC} - d_{\rm rej}$

  $i = i_{\rm next}$

  $\boldsymbol{e}_{\rm EC} = \boldsymbol{e}_{\rm EC,next}$

- **Repeat until** $\ell_{\rm EC} = 0$

- Rotate active forces:

  for each particle i

  $\langle \Delta t_{EC}\rangle_i = \frac{d_i}{\ell_{EC}}\langle \Delta t_{\rm EC}\rangle$

  $\theta_i \mathrel{+}= \text{ Gauss}(0, \sqrt{2D_r\langle t_{EC}\rangle_i})$

  $d_i = 0$

- Loop back to beginning

Here rand(...) is a uniformly distributed and Gauss(...) is a Gaussian distributed random number.

B. Mean ECMC move vector $\langle \Delta \boldsymbol{r}_{\rm EC}\rangle$ for a single particle

We consider a single particle under a constant force $F_0\boldsymbol{e}$ and calculate its mean move vector $\langle \Delta \boldsymbol{r}_{\rm EC}\rangle$ during one algorithmic ECMC step. The ECMC algorithm draws a random direction $\boldsymbol{e}_{\rm EC}$ and moves the particle by the EC length $\ell_{\rm EC}$. We introduce the angle ϕ between the unit propulsion direction vector $\boldsymbol{e}$ and the EC unit vector $\boldsymbol{e}_{\rm EC}$ by $\cos\phi \equiv \boldsymbol{e}_{\rm EC}\cdot\boldsymbol{e}$. The mean move vector $\langle \Delta \boldsymbol{r}_{\rm EC}\rangle$ will be averaged over all angles ϕ, i.e., over all EC directions because EC directions are chosen randomly in the algorithm and we are interested in the mean algorithmic displacement over many ECMC moves. Three cases have to be considered in the calculation of $\langle \Delta \boldsymbol{r}_{\rm EC}\rangle$ depending on ϕ and $\ell_{\rm EC}$, and we have to properly average over these cases and all angles ϕ.

(i) If $\cos\phi \geq 0$, the move is energetically downhill. Then the particle is displaced by the full EC length $\ell_{\rm EC}$ resulting in a mean displacement

$$\langle \Delta \boldsymbol{r}_{\rm EC}\rangle_{\cos\phi\geq 0} = \ell_{\rm EC}\boldsymbol{e}_{\rm EC} \tag{1}$$

for given ϕ. Averaging over all angles $\phi \in [-\pi/2, \pi/2]$ with $\cos\phi \geq 0$, we obtain

$$\begin{aligned}\langle \Delta \boldsymbol{r}_{\rm EC}\rangle_{\geq} &= \frac{1}{\pi}\int_{-\pi/2}^{\pi/2} {\rm d}\phi \langle \Delta \boldsymbol{r}_{\rm EC}\rangle_{\cos\phi\geq 0} \\ &= \frac{1}{\pi}\ell_{\rm EC}\int_{-\pi/2}^{\pi/2}{\rm d}\phi\cos\phi\boldsymbol{e} = \frac{2}{\pi}\ell_{\rm EC}\boldsymbol{e}. \end{aligned} \tag{2}$$

(ii) If $\cos\phi < 0$, the move is energetically uphill and a "usable" energy $\Delta U > 0$ for uphill motion is drawn from an exponential Boltzmann distribution $p(\Delta U) \sim \exp(-\beta\Delta U)$ ($\beta = 1/k_{\rm B}T$) and a rejection distance $d_{\rm rej}$ is determined from $\Delta U = F_0 d_{\rm rej}|\cos\phi|$. This is equivalent to drawing the rejection distance from an exponential distribution

$$p_d(d_{\rm rej}) = \beta F_0|\cos\phi| e^{-\beta F_0 d_{\rm rej}|\cos\phi|}. \tag{3}$$

Now, two subcases arise:

(iia) $d_{\rm rej} \geq \ell_{\rm EC}$, where the particle is moved by the full event chain length, $\Delta\boldsymbol{r} = \ell_{\rm EC}\boldsymbol{e}_{\rm EC}$. This happens with probability

$$p_> = \int_{\ell_{\rm EC}}^{\infty} dx p_d(x) = e^{-\beta F_0\ell_{\rm EC}|\cos\phi|}. \tag{4}$$

This subcase will give the dominating contribution in the limit $\beta F_0\ell_{\rm EC} \ll 1$ of small EC lengths or weak propulsion forces.

(iib) $d_{\rm rej} < \ell_{\rm EC}$, where the particle is only moved by $\Delta\boldsymbol{r} = d_{\rm rej}\boldsymbol{e}_{\rm EC}$. Then, the EC direction is lifted $\boldsymbol{e}_{\rm EC} \to \boldsymbol{e}'_{\rm EC}$ by reflecting with respect to the equipotential surface, $\boldsymbol{e}'_{\rm EC} = \boldsymbol{e}_{\rm EC} - 2\cos\phi\boldsymbol{e}$. In total, this results in $\Delta\boldsymbol{r} = d_{\rm rej}\boldsymbol{e}_{\rm EC} + (\ell_{\rm EC} - d_{\rm rej})\boldsymbol{e}'_{\rm EC}$. This displacement is realized with probability $p_d(d_{\rm rej})$. This subcase will give the dominating contribution in the limit $\beta F_0\ell_{\rm EC} \gg 1$ of large EC lengths or strong propulsion forces.

Averaging over $p_d(d_{\rm rej})$ we obtain for the mean vectorial displacement

$$\begin{aligned}&\langle \Delta \boldsymbol{r}_{\rm EC}\rangle_{\cos\phi<0} \\ &= p_>\ell_{\rm EC}\boldsymbol{e}_{\rm EC} + \int_0^{\ell_{\rm EC}} dx p_d(x)\left[x\boldsymbol{e}_{\rm EC} + (\ell_{\rm EC}-x)\boldsymbol{e}'_{\rm EC}\right] \\ &= p_>\ell_{\rm EC}\boldsymbol{e}_{\rm EC} \\ &\quad + \int_0^{\ell_{\rm EC}} dx p_d(x)\left[\ell_{\rm EC}\boldsymbol{e}_{\rm EC} - 2\cos\phi(\ell_{\rm EC}-x)\boldsymbol{e}\right] \\ &= \ell_{\rm EC}\boldsymbol{e}_{\rm EC} \\ &\quad - 2\cos\phi\boldsymbol{e}\int_0^{\ell_{\rm EC}} dx p_d(x)(\ell_{\rm EC}-x) \\ &= \ell_{\rm EC}\boldsymbol{e}_{\rm EC} \\ &\quad - \boldsymbol{e}\frac{2}{\beta F_0}\left(1 - \beta F_0\ell_{\rm EC}|\cos\phi| - e^{-\beta F_0\ell_{\rm EC}|\cos\phi|}\right) \end{aligned} \tag{5}$$

for given ϕ. Averaging over the all angles $\phi \in [\pi/2, 3\pi/2]$ with $\cos\phi < 0$, we obtain

$$\begin{aligned}&\langle \Delta \boldsymbol{r}_{\rm EC}\rangle_{<} \\ &= -\frac{1}{\pi}\ell_{\rm EC}\int_{-\pi/2}^{\pi/2}{\rm d}\phi\cos\phi\boldsymbol{e} \\ &\quad - \boldsymbol{e}\frac{2}{\beta F_0}\frac{1}{\pi}\int_{-\pi/2}^{\pi/2}{\rm d}\phi\left(1 - \beta F_0\ell_{\rm EC}|\cos\phi| - e^{-\beta F_0\ell_{\rm EC}|\cos\phi|}\right) \\ &= \frac{2}{\pi}\ell_{\rm EC}\boldsymbol{e} - \frac{2}{\beta F_0}\frac{1}{\pi}\int_{-\pi/2}^{\pi/2}{\rm d}\phi\left(1 - e^{-\beta F_0\ell_{\rm EC}|\cos\phi|}\right)\boldsymbol{e} \end{aligned} \tag{6}$$

Averaging over the two cases $\cos\phi \geq 0$ and $\cos\phi < 0$, we finally obtain

$$\begin{aligned}\langle \Delta \boldsymbol{r}_{\mathrm{EC}} \rangle &= \frac{1}{2}\left(\langle \Delta \boldsymbol{r}_{\mathrm{EC}} \rangle_{\geq} + \langle \Delta \boldsymbol{r}_{\mathrm{EC}} \rangle_{<}\right) \\ \frac{\langle \Delta \boldsymbol{r}_{\mathrm{EC}} \rangle}{\ell_{\mathrm{EC}}} &= \frac{2}{\pi}\boldsymbol{e} \\ &\quad - \frac{1}{\beta F_0 \ell_{\mathrm{EC}}}\frac{1}{\pi}\int_{-\pi/2}^{\pi/2} \mathrm{d}\phi \left(1 - e^{-\beta F_0 \ell_{\mathrm{EC}} |\cos\phi|}\right)\boldsymbol{e} \\ &= x f(x) \boldsymbol{e} \end{aligned} \tag{7}$$

with

$$x \equiv \beta F_0 \ell_{\mathrm{EC}} = v_0 \ell_{\mathrm{EC}}/D = 3\mathrm{Pe}\ell_{\mathrm{EC}}/\sigma \tag{8}$$

and a scaling function

$$f(x) = \frac{2}{\pi}\frac{1}{x} - \frac{1}{x^2}\frac{1}{\pi}\int_{-\pi/2}^{\pi/2} d\phi (1 - e^{-x\cos\phi}) \tag{9}$$

as in Eq. (5equation.2.5) in the main text. It is also apparent that the projected mean EC move length is simply related via

$$\langle \Delta \boldsymbol{r}_{\mathrm{EC}} \cdot \boldsymbol{e} \rangle = \langle \Delta \boldsymbol{r}_{\mathrm{EC}} \rangle \cdot \boldsymbol{e}. \tag{10}$$

The function $f(x)$ has the limiting behaviors $f(x) \approx 1/4 - 2x/9\pi$ for $x \ll 1$ (in the limit $\beta F_0 \ell_{\mathrm{EC}} \ll 1$ of small EC lengths or weak propulsion forces) and $f(x) \approx 2/\pi x - 1/x^2$ for $x \gg 1$ (in the limit $\beta F_0 \ell_{\mathrm{EC}} \gg 1$ of large EC lengths or strong propulsion forces). Figure 1 shows perfect agreement of the analytically calculated scaling function $f(x)$ with the kEC simulation.

The limiting cases $x \ll 1$ and $x \gg 1$ differ in their behaviour under an opposing force ($\cos\phi < 0$). For $x \ll 1$, the particle moves with probability $p_>$ the whole EC length against a weak opposing force resulting in $\langle \Delta \boldsymbol{r}_{\mathrm{EC}} \rangle_{\cos\phi<0} \approx p_> \ell_{\mathrm{EC}} \boldsymbol{e}_{\mathrm{EC}} = e^{-\beta F_0 \ell_{\mathrm{EC}} |\cos\phi|} \ell_{\mathrm{EC}} \boldsymbol{e}_{\mathrm{EC}}$ (corrections from lifting and reflection are of order F_0^2), while $\langle \Delta \boldsymbol{r}_{\mathrm{EC}} \rangle_{\cos\phi\geq 0} = \ell_{\mathrm{EC}} \boldsymbol{e}_{\mathrm{EC}}$ for a move in the opposite direction $-\boldsymbol{e}_{\mathrm{EC}}$. This leads to exactly the same behaviour as in a local MC algorithm for a local MC move of length ℓ_{EC} in directions $\pm\boldsymbol{e}_{\mathrm{EC}}$ under the standard Metropolis rule fulfilling detailed balance, thus establishing equivalence to local Metropolis MC in the limit of small EC lengths ℓ_{EC}. After expanding in $x \ll 1$ and averaging over all directions this gives $\langle \Delta \boldsymbol{r}_{\mathrm{EC}} \rangle \approx (1/4)\beta F_0 \ell_{\mathrm{EC}}^2 \boldsymbol{e}$.

For $x \gg 1$, on the other hand, the particle is lifted after a short mean distance $1/\beta F_0 |\cos\phi|$ in direction against a strong opposing force and reflected. Essentially, this results in a move in the reflected direction over the whole EC length, $\langle \Delta \boldsymbol{r}_{\mathrm{EC}} \rangle_{\cos\phi<0} \approx \ell_{\mathrm{EC}} \boldsymbol{e}_{\mathrm{EC}} + 2|\cos\phi| \ell_{\mathrm{EC}} \boldsymbol{e}$. After averaging over all directions this gives $\langle \Delta \boldsymbol{r}_{\mathrm{EC}} \rangle_{<} \approx -(2/\pi)\ell_{\mathrm{EC}} \boldsymbol{e} + (4/\pi)\ell_{\mathrm{EC}} \boldsymbol{e}$ resulting in $\langle \Delta \boldsymbol{r}_{\mathrm{EC}} \rangle \approx (2/\pi)\ell_{\mathrm{EC}} \boldsymbol{e}$.

In practice, the following fit function for $f(x)$ is useful to interpolate between both limiting cases (see also Fig. 1):

$$f(x) = \frac{1}{ax + b\sqrt{x} + c} \tag{11}$$

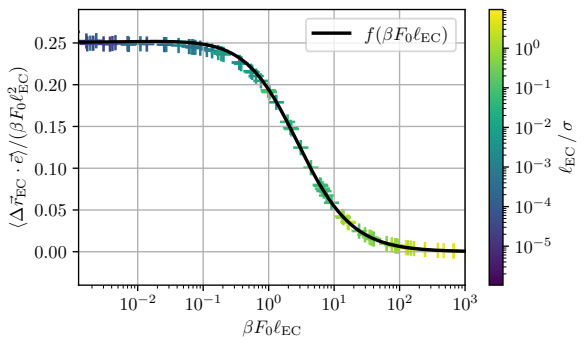

FIG. 1. Mean ECMC move lengths in force direction $\langle \Delta \boldsymbol{r}_{\mathrm{EC}} \cdot \boldsymbol{e} \rangle$ in units of $\beta F_0 \ell_{\mathrm{EC}}^2$ as a function of $x = \beta F_0 \ell_{\mathrm{EC}}$. The kEC simulation data (crosses) for different EC lengths ℓ_{EC} (color-coded) collapse onto the analytically calculated scaling function $f(x)$ from Eq. (5equation.2.5) in the main text and Eqs. (7) and (10) (black line, to reduce the computational effort the fit function (11) is plotted).

with $a = \pi/2$, $b = -0.42$, and $c = 4$, which is constructed to satisfy the limits $f(x) \approx 1/4$ for $x \approx 0$ and $f(x) \approx 2/\pi x$ for $x \to \infty$, so that b is the only free parameter. This fit function can be used to speed up calculations in production runs.

C. Mean square and mean cubic ECMC move lengths for a single particle

Following similar steps, we can also calculate the mean square and mean cubic move lengths $\langle (\Delta \boldsymbol{r}_{\mathrm{EC}} \cdot \boldsymbol{e})^2 \rangle$, $\langle (\Delta \boldsymbol{r}_{\mathrm{EC}} \cdot \boldsymbol{e})^3 \rangle$ and $\langle (\Delta \boldsymbol{r}_{\mathrm{EC}})^2 \rangle$ during one algorithmic ECMC step. In the following we use $x \equiv \beta F_0 \ell_{\mathrm{EC}}$ from Eq. (8).

1. *Derivation of* $\langle (\Delta \boldsymbol{r}_{\mathrm{EC}} \cdot \boldsymbol{e})^2 \rangle$

If $\cos\phi \geq 0$:

$$\frac{\langle (\Delta \boldsymbol{r}_{\mathrm{EC}} \cdot \boldsymbol{e})^2 \rangle_{\cos\phi\geq 0}}{\ell_{\mathrm{EC}}^2} = \cos^2\phi \tag{12}$$

$$\frac{\langle (\Delta \boldsymbol{r}_{\mathrm{EC}} \cdot \boldsymbol{e})^2 \rangle_{\geq}}{\ell_{\mathrm{EC}}^2} = \frac{1}{2}. \tag{13}$$

If $\cos\phi < 0$:

$$\frac{\langle(\Delta \boldsymbol{r}_{\mathrm{EC}}\cdot\boldsymbol{e})^2\rangle_{cos\phi<0}}{\ell_{\mathrm{EC}}^2} = (\cos\phi)^2 - \frac{4}{x^2}\Big(x|\cos\phi| - 2 + \big(x|\cos\phi|+2\big)e^{-x|\cos\phi|}\Big) \quad (14)$$

$$\frac{\langle(\Delta \boldsymbol{r}_{\mathrm{EC}}\cdot\boldsymbol{e})^2\rangle_{<}}{\ell_{\mathrm{EC}}^2} = \frac{1}{2} - \frac{4}{\pi x^2}\int_{-\pi/2}^{\pi/2}\mathrm{d}\phi\,\Big(x|\cos\phi| - 2 + \big(x|\cos\phi|+2\big)e^{-x|\cos\phi|}\Big). \quad (15)$$

The final result after averaging over the two cases $\cos\phi \geq 0$ and $\cos\phi < 0$ is

$$\frac{\langle(\Delta \boldsymbol{r}_{\mathrm{EC}}\cdot\boldsymbol{e})^2\rangle}{\ell_{\mathrm{EC}}^2} = \frac{1}{2} - \frac{2}{\pi x^2}\int_{-\pi/2}^{\pi/2}\mathrm{d}\phi\,\Big(x|\cos\phi| - 2 + \big(x|\cos\phi|+2\big)e^{-x|\cos\phi|}\Big). \quad (16)$$

2. Derivation of $\langle(\Delta \boldsymbol{r}_{\mathrm{EC}})^2\rangle$

If $\cos\phi \geq 0$:

$$\frac{\langle(\Delta \boldsymbol{r}_{\mathrm{EC}})^2\rangle_{\cos\phi\geq 0}}{\ell_{\mathrm{EC}}^2} = 1 \quad (17)$$

$$\frac{\langle(\Delta \boldsymbol{r}_{\mathrm{EC}})^2\rangle_{\geq}}{\ell_{\mathrm{EC}}^2} = 1. \quad (18)$$

If $\cos\phi < 0$:

$$\frac{\langle(\Delta \boldsymbol{r}_{\mathrm{EC}})^2\rangle_{\cos\phi<0}}{\ell_{\mathrm{EC}}^2} = 1 - \frac{4}{x^2}\Big(x|\cos\phi| - 2 + \big(x|\cos\phi|+2\big)e^{-x|\cos\phi|}\Big) \quad (19)$$

$$\frac{\langle(\Delta \boldsymbol{r}_{\mathrm{EC}})^2\rangle_{<}}{\ell_{\mathrm{EC}}^2} = 1 - \frac{4}{\pi x^2}\int_{-\pi/2}^{\pi/2}\mathrm{d}\phi\,\Big(x|\cos\phi| - 2 + \big(x|\cos\phi|+2\big)e^{-x|\cos\phi|}\Big). \quad (20)$$

The final result after averaging over the two cases $\cos\phi \geq 0$ and $\cos\phi < 0$ is

$$\frac{\langle(\Delta \boldsymbol{r}_{\mathrm{EC}})^2\rangle}{\ell_{\mathrm{EC}}^2} = 1 - \frac{2}{\pi x^2}\int_{-\pi/2}^{\pi/2}\mathrm{d}\phi\,\Big(x|\cos\phi| - 2 + \big(x|\cos\phi|+2\big)e^{-x|\cos\phi|}\Big). \quad (21)$$

We find $\langle(\Delta \boldsymbol{r}_{\mathrm{EC}})^2\rangle/\ell_{\mathrm{EC}}^2 \approx 1$ both in the limits $x \gg 1$ and $x \ll 1$, see also Fig. 2 (bottom, orange line).

3. Derivation of $\langle(\Delta \boldsymbol{r}_{\mathrm{EC}}\cdot\boldsymbol{e})^3\rangle$

If $\cos\phi \geq 0$:

$$\frac{\langle(\Delta \boldsymbol{r}_{\mathrm{EC}}\cdot\boldsymbol{e})^3\rangle_{\cos\geq 0}}{\ell_{\mathrm{EC}}^3} = \cos^3\phi \quad (22)$$

$$\frac{\langle(\Delta \boldsymbol{r}_{\mathrm{EC}}\cdot\boldsymbol{e})^3\rangle_{\geq}}{\ell_{\mathrm{EC}}^3} = \frac{4}{3\pi}. \quad (23)$$

If $\cos\phi < 0$:

$$\frac{\langle(\Delta \boldsymbol{r}_{\mathrm{EC}}\cdot\boldsymbol{e})^3\rangle_{\cos<0}}{\ell_{\mathrm{EC}}^3} = \cos^3\phi(A+B-1) \quad (24)$$

$$\frac{\langle(\Delta \boldsymbol{r}_{\mathrm{EC}}\cdot\boldsymbol{e})^3\rangle_{<}}{\ell_{\mathrm{EC}}^3} = \frac{1}{\pi}\int_{\pi/2}^{3\pi/2}\mathrm{d}\phi\,\frac{\langle(\Delta \boldsymbol{r}_{\mathrm{EC}}\cdot\boldsymbol{e})^3\rangle_{\cos<0}}{\ell_{\mathrm{EC}}^3} \quad (25)$$

using

$$A = \frac{1}{x^3|\cos\phi|^3}\Big(6x^2|\cos\phi|^2 - 24x|\cos\phi| + 48\Big) \quad (26)$$

$$B = -\frac{\exp(-x|\cos\phi|)}{x^3|\cos\phi|^3}\Big(6x^2|\cos\phi|^2 + 24x|\cos\phi| + 48\Big). \quad (27)$$

The final result after averaging over the two cases

$$\frac{\langle(\Delta \boldsymbol{r}_{\mathrm{EC}}\cdot\boldsymbol{e})^3\rangle}{\ell_{\mathrm{EC}}^3} = \frac{1}{2\pi}\int_{\pi/2}^{3\pi/2}\mathrm{d}\phi\,\cos^3\phi(A+B-2). \quad (28)$$

II. VALIDATION OF THE KEC ALGORITHM

A. One-body problem: the kEC algorithm becomes exact for small ℓ_{EC}

We assign a kEC simulation time $\langle\Delta t_{\mathrm{EC}}\rangle$ to each particle according to the relation $\langle\Delta \boldsymbol{r}\cdot\boldsymbol{e}\rangle = v_0\Delta t$ for the *first* moment of the displacement in force direction, which holds exactly for single free ABPs by requiring that $\langle\Delta \boldsymbol{r}_{\mathrm{EC}}\cdot\boldsymbol{e}\rangle = v_0\langle\Delta t_{\mathrm{EC}}\rangle$ (see main text and preceding section). This procedure works equally well for all EC lengths ℓ_{EC} as demonstrated in Fig. 1 and, thus, does not single out an optimal EC length. An optimal EC length could emerge if we also consider *higher* moments $\langle(\Delta \boldsymbol{r}\cdot\boldsymbol{e})^n\rangle$ of the displacement in force direction as a function of Δt and require that analytical results for ABPs also hold for the higher moments if we use $\Delta \boldsymbol{r}_{\mathrm{EC}}$ for the displacement and $\langle\Delta t_{\mathrm{EC}}\rangle$ for Δt.

Simple exact analytical results for these higher moments for single free ABPs are not available, but approximate results which hold in the short time limit $\Delta t \ll \tau$:

$$\langle(\Delta \boldsymbol{r}\cdot\boldsymbol{e})^2\rangle \approx (v_0\Delta t)^2 + 2D\Delta t, \quad (29)$$

$$\langle(\Delta \boldsymbol{r}\cdot\boldsymbol{e})^3\rangle \approx (v_0\Delta t)^3 + 6v_0D\Delta t^2, \quad (30)$$

$$\langle\Delta \boldsymbol{r}^2\rangle \approx (v_0\Delta t)^2 + 4D\Delta t. \quad (31)$$

We have calculated the algorithmic counterpart of the left hand sides of Eqs. 29-31 in Sec. I C for one ECMC

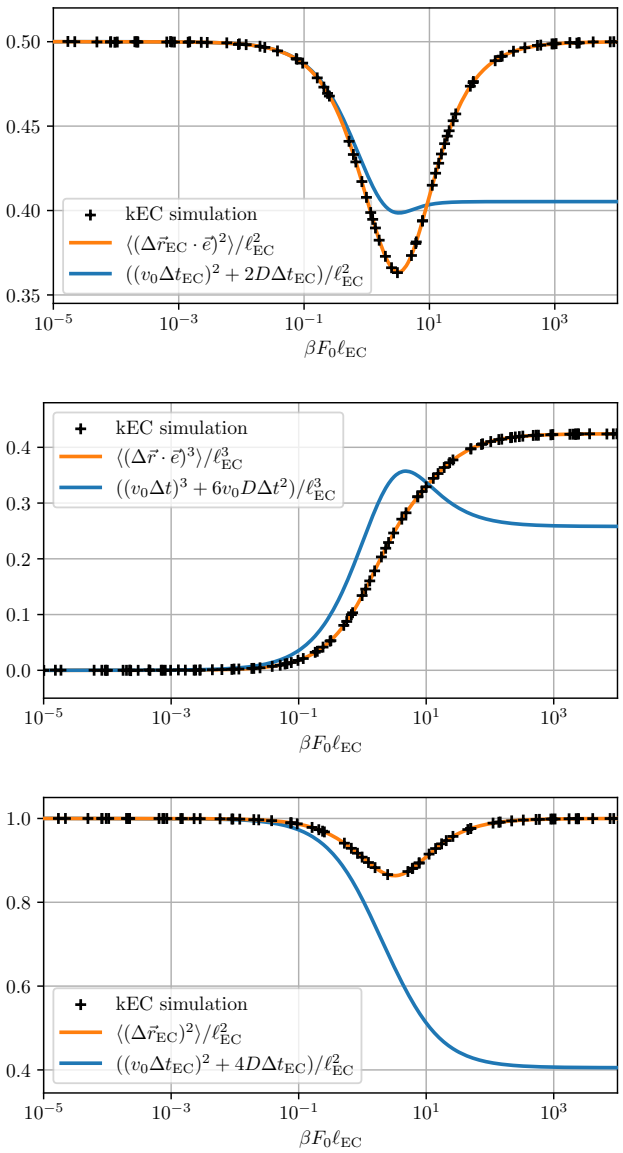

FIG. 2. Higher moments of the ECMC move lengths (left-hand sides of Eqs. 29 - 31) normalized to the n-th power of the EC length $\ell_{\rm EC}$ as a function of $x=\beta F_0\ell_{\rm EC}$. The kEC simulation data (black crosses) agree with analytical calculations (orange lines). Left and right hand sides of Eqs. 29 - 31 evaluated with $\Delta t=\langle\Delta t_{\rm EC}\rangle$ (blue lines) agree with the orange lines in the limit $\beta F_0\ell_{\rm EC}\to 0$, indicating that the limit $v_0\ell_{\rm EC}/D\to 0$ reproduces correct physical behaviour on a single step level.

move analytically. Figure 2 shows $\langle(\Delta\boldsymbol{r}_{\rm EC}\cdot\boldsymbol{e})^2\rangle/\ell_{\rm EC}^2$, $\langle(\Delta\boldsymbol{r}_{\rm EC}\cdot\boldsymbol{e})^3\rangle/\ell_{\rm EC}^3$ and $\langle\Delta\boldsymbol{r}_{\rm EC}^2\rangle/\ell_{\rm EC}^2$ as a function of the dimensionless parameter $x=\beta F_0\ell_{\rm EC}$ and demonstrates perfect agreement between these analytical calculations (orange lines) and kEC simulation data (black crosses). Note that all analytical results of Sec. I C only depend on the parameter x.

It is not obvious whether or not Eqs. 29-31 for higher moments are valid within the kEC algorithm using the corresponding mean time per EC step $\Delta t=\langle\Delta t_{\rm EC}\rangle$. For this reason Fig. 2 also shows the right hand sides of Eqs. 29-31 for $\Delta t=\langle\Delta t_{\rm EC}\rangle$ (blue lines). We expect the approximations in Eqs. 29 - 31 to break down for $\Delta t=\langle\Delta t_{\rm EC}\rangle>\tau$. This is equivalent to $x>(3\pi/2){\rm Pe}^2$ for high activity ${\rm Pe}>1$ (and $x\ll 2\sqrt{3}{\rm Pe}$ in the passive limit ${\rm Pe}\ll 1$), see main text. Numerically, we find the values of Δt, at which the approximations in Eqs. 29-31 break down (= relative error of at least 5% to the exact result), correspond - for all relevant active forces - to values of $x>x_c=10^1-10^4$. In other words: the origin of the deviations in Fig. 2 between the blue and orange lines are *not* a result of the approximations in Eqs. 29-31 itself but are solely algorithmic for $x<x_c$, i.e., due to a failure of our choice $\Delta t=\langle\Delta t_{\rm EC}\rangle$ for a timestep.

Figure 2 shows that these algorithmic deviations between left hand and right hand sides of Eqs. 29-31 (orange and blue lines, respectively) become large for $x=\beta F_0\ell_{\rm EC}>1-10$. For an optimal EC lengths $\ell_{\rm EC}$, we would require left hand and right hand sides to exhibit a common intersection at a corresponding optimal x-value. Since there are no common intersections, we are unable to determine a *perfect* EC length, which would reproduce all quantities related to the equations of motion correctly on a single particle level. However, in accordance with the observations made in the main text, all deviations in Fig. 2 vanish for *small* $x=\beta F_0\ell_{\rm EC}\ll 10^{-1}$. This implies that all of those one-particle single-step quantities are correctly reproduced in the limit $\ell_{\rm EC}/\sigma=x/3{\rm Pe}\to 0$. More generally, we will derive that, for a single ABP, the kEC algorithm converges to the correct one-particle Fokker-Planck equation in the limit of vanishing EC lengths in the following section.

B. The one-particle Fokker-Planck equation for the kEC algorithm converges to the ABP Fokker-Planck equation for small $\ell_{\rm EC}$

The stochastic motion of a single free ABP can be completely captured by the one-particle Fokker-Planck equation for the probability density $P(\boldsymbol{r},\theta,t)$ to find the particle at position $\boldsymbol{r}$ with orientation θ at time t,

$$\partial_t P(\boldsymbol{r},\theta,t)\approx -(v_0\boldsymbol{e})\cdot\boldsymbol{\nabla}_{\boldsymbol{r}}P(\boldsymbol{r},\theta,t)+D_r\partial_\theta^2 P(\boldsymbol{r},\theta,t)+D\boldsymbol{\nabla}_{\boldsymbol{r}}^2P(\boldsymbol{r},\theta,t),\tag{32}$$

In the following we will show that the kEC algorithm converges to the same one-particle Fokker-Planck equation in the limit of vanishing EC lengths or small timesteps $\Delta t=\langle\Delta t_{\rm EC}\rangle$. As a result, *all* moments $\langle(\Delta\boldsymbol{r}\cdot\boldsymbol{e})^n\rangle$ of the displacement as a function of Δt are correctly reproduced in this limit further generalizing the results of the previous sections.

Let $P(\boldsymbol{r},\theta,t)$ be the probability density to find the particle at $(\boldsymbol{r},\theta)$ at time t and $p_\phi(\boldsymbol{r}|\boldsymbol{r}',\theta|\theta')$ the probability density to transition from $\boldsymbol{r}'$ to $\boldsymbol{r}$ and from θ' to θ within

one step of the kEC algorithm with EC direction $\boldsymbol{e}_{\mathrm{EC}}$. The EC direction is given by the angle ϕ with the unit propulsion direction vector $\boldsymbol{e}$. We average $P(\boldsymbol{r},\theta,t)$ over all angles ϕ, i.e., over all EC directions in each kEC step until time t. The probability density $P(\boldsymbol{r},\theta,t+\langle\Delta t_{\mathrm{EC}}\rangle)$ one kEC timestep later can be related to $P(\boldsymbol{r},\theta,t)$ via

$$\begin{aligned}&P(\boldsymbol{r},\theta,t+\langle\Delta t_{\mathrm{EC}}\rangle)\\&=\frac{1}{2\pi}\int_0^{2\pi}d\phi\int_V d^2\boldsymbol{r}'\int_{-\infty}^{\infty}d\theta' p_\phi(\boldsymbol{r}|\boldsymbol{r}',\theta|\theta')P(\boldsymbol{r}',\theta',t),\end{aligned}\tag{33}$$

where we average over all angles ϕ also in the last kEC step. The average time corresponding to one kEC step $\langle\Delta t_{\mathrm{EC}}\rangle$; we will see in the course of our derivation of the Fokker-Planck equation how the algorithmic timestep $\langle\Delta t_{\mathrm{EC}}\rangle$ has to be chosen to arrive at the ABP Fokker-Planck equation (32). Analogously to the standard derivation of Fokker-Planck equations, we can argue that the transition probability $p_\phi(\boldsymbol{r}|\boldsymbol{r}',\theta|\theta')$ for a single kEC timestep is peaked around $\theta=\theta'$ and, typically, $|\boldsymbol{r}-\boldsymbol{r}'|\sim\ell_{\mathrm{EC}}$ for one kEC step. We will consider the limit of small ℓ_{EC} and will neglect variations on scales $|\boldsymbol{r}-\boldsymbol{r}'|\lesssim\ell_{\mathrm{EC}}$. Therefore, we can expand $P(\boldsymbol{r}',\theta',t)$ in $\boldsymbol{r}'$ and θ' around $\boldsymbol{r}$ and θ to obtain

$$\begin{aligned}&P(\boldsymbol{r},\theta,t+\langle\Delta t_{\mathrm{EC}}\rangle)\\&\approx P(\boldsymbol{r},\theta,t)+\frac{1}{2\pi}\int_0^{2\pi}d\phi\int_V d^2\boldsymbol{r}'\int_{-\infty}^{\infty}d\theta' p_\phi(\boldsymbol{r}|\boldsymbol{r}',\theta|\theta')\times\\&\Big(-\boldsymbol{\nabla}_{\boldsymbol{r}}P(\boldsymbol{r},\theta,t)\cdot(\boldsymbol{r}-\boldsymbol{r}')\\&+\frac{1}{2}\sum_{i,j=1}^{2}\partial_{r_i}\partial_{r_j}P(\boldsymbol{r},\theta,t)(r_i-r_i')(r_j-r_j')\\&-\partial_\theta P(\boldsymbol{r},\theta,t)(\theta-\theta')+\frac{1}{2}\partial_\theta^2P(\boldsymbol{r},\theta,t)(\theta-\theta')^2\Big)\\&=P(\boldsymbol{r},\theta,t)-\boldsymbol{\nabla}_{\boldsymbol{r}}P(\boldsymbol{r},\theta,t)\cdot\langle\Delta\boldsymbol{r}_{\mathrm{EC}}\rangle\\&+\frac{1}{2}\partial_x^2P(\boldsymbol{r},\theta,t)\langle\Delta x_{\mathrm{EC}}^2\rangle+\frac{1}{2}\partial_y^2P(\boldsymbol{r},\theta,t)\langle\Delta y_{\mathrm{EC}}^2\rangle\\&-\partial_\theta P(\boldsymbol{r},\theta,t)\langle\Delta\theta_{\mathrm{EC}}\rangle+\frac{1}{2}\partial_\theta^2P(\boldsymbol{r},\theta,t)\langle\Delta\theta_{\mathrm{EC}}^2\rangle.\end{aligned}\tag{34}$$

For our kEC algorithm the transition probability factorizes, $p_\phi(\boldsymbol{r}|\boldsymbol{r}',\theta|\theta')=f_\phi(\boldsymbol{r}|\boldsymbol{r}')g(\theta|\theta')$ because, after each ECMC move, the angular change $\Delta\theta$ is drawn from a Gaussian distribution with zero mean $\langle\Delta\theta_{\mathrm{EC}}\rangle=0$ and and variance $\langle\Delta\theta_{\mathrm{EC}}^2\rangle=2D_r\langle\Delta t_{\mathrm{EC}}\rangle$ independently of the ECMC move vector. Therefore, there are no mixed terms in the Taylor expansion (34). We can specify the spatial transition probability as

$$f_\phi(\boldsymbol{r}|\boldsymbol{r}')|_{\cos\phi\geq0}=\delta\big(\boldsymbol{r}-(\boldsymbol{r}'+\ell_{\mathrm{EC}}\boldsymbol{e}_{\mathrm{EC}})\big)\tag{35}$$

for $\cos\phi\geq0$ and

$$\begin{aligned}f_\phi(\boldsymbol{r}|\boldsymbol{r}')|_{\cos\phi<0}=\int_0^{\ell_{\mathrm{EC}}}&\mathrm{d}x p_d(x)\times\\&\delta\big(\boldsymbol{r}-(\boldsymbol{r}'+\ell_{\mathrm{EC}}\boldsymbol{e}_{\mathrm{EC}}-2\cos\phi(\ell_{\mathrm{EC}}-x)\boldsymbol{e})\big)\\&+\delta\big(\boldsymbol{r}-(\boldsymbol{r}'+\ell_{\mathrm{EC}}\boldsymbol{e}_{\mathrm{EC}})\big)e^{-\beta F_a\ell_{\mathrm{EC}}|\cos\phi|}\end{aligned}\tag{36}$$

for $\cos\phi<0$ with $p_d(x)$ previously defined in Eq. (3). Therefore, the transition probability $p_\phi(\boldsymbol{r}|\boldsymbol{r}',\theta|\theta')$ for a single kEC timestep is Gaussian in the angle θ and peaked around $\theta=\theta'$ but, obviously, not Gaussian in $\boldsymbol{r}$ due to the deterministic nature of EC moves. Nevertheless, also the above results for $f_\phi(\boldsymbol{r}|\boldsymbol{r}')$ are peaked around $|\boldsymbol{r}-\boldsymbol{r}'|\sim\ell_{\mathrm{EC}}$ for one kEC step as assumed in the Taylor expansion in Eq. (34).

The Taylor expansion in θ is justified if $\langle\Delta\theta_{\mathrm{EC}}^2\rangle\ll1$ or $\langle\Delta t_{\mathrm{EC}}\rangle\ll1/D_r=\tau$. This is exactly the condition of smooth rotation discussed in the main text. If this condition is fulfilled we can also neglect higher orders of the Taylor expansion in θ because $\langle\Delta\theta_{\mathrm{EC}}^{2n}\rangle\sim(D_r\langle\Delta t_{\mathrm{EC}}\rangle)^n$. Typically this is a relatively weak condition requiring only moderately small EC lengths $\ell_{\mathrm{EC}}/\sigma\ll(\pi/2)\mathrm{Pe}$ for high activity $\mathrm{Pe}>1$. In Eq. (34), we also neglected higher orders of the Taylor expansion in $\boldsymbol{r}$ because $\langle\Delta r_{i,\mathrm{EC}}^n\rangle\sim\ell_{\mathrm{EC}}^n$ will be justified by the requirement of small EC lengths.

Further approximating $\partial_tP(\boldsymbol{r},\theta,t)\approx(P(\boldsymbol{r},\theta,t+\langle\Delta t_{\mathrm{EC}}\rangle)-P(\boldsymbol{r},\theta,t))/\langle\Delta t_{\mathrm{EC}}\rangle$ and using

$$\langle\Delta x_{\mathrm{EC}}^2\rangle=\langle\Delta y_{\mathrm{EC}}^2\rangle\approx\frac{1}{2}\ell_{\mathrm{EC}}^2\quad(x\ll1).\tag{37}$$

for the second moments of the ECMC move length (see Sec. I C), we obtain

$$\begin{aligned}\partial_tP(\boldsymbol{r},\theta,t)\approx&-\boldsymbol{\nabla}_{\boldsymbol{r}}P(\boldsymbol{r},\theta,t)\cdot\frac{\langle\Delta\boldsymbol{r}_{\mathrm{EC}}\rangle}{\langle\Delta t_{\mathrm{EC}}\rangle}\\&+\boldsymbol{\nabla}_{\boldsymbol{r}}^2P(\boldsymbol{r},\theta,t)\frac{\ell_{\mathrm{EC}}^2}{4\langle\Delta t_{\mathrm{EC}}\rangle}\\&+D_r\partial_\theta^2P(\boldsymbol{r},\theta,t).\end{aligned}\tag{38}$$

At this point, we see that the algorithmic timestep $\langle\Delta t_{\mathrm{EC}}\rangle$ has to be chosen as

$$\langle\Delta\boldsymbol{r}_{\mathrm{EC}}\rangle=\boldsymbol{v}_0\langle\Delta t_{\mathrm{EC}}\rangle\tag{39}$$

for the convective term to agree with the ABP Fokker-Planck equation (32). This is exactly our definition of the mean time $\langle\Delta t_{\mathrm{EC}}\rangle$ from the main text. Finally, if also the diffusive term is required to agree with the ABP Fokker-Planck equation (32), we need

$$\frac{\ell_{\mathrm{EC}}^2}{4\langle\Delta t_{\mathrm{EC}}\rangle}\approx D.\tag{40}$$

This poses a relatively strong condition and is only fulfilled for $x\ll1$ or small EC lengths $\ell_{\mathrm{EC}}/\sigma\ll1/3\mathrm{Pe}$. For $x>1$, the apparent translational diffusion constant $D'=\ell_{\mathrm{EC}}^2/4\langle\Delta t_{\mathrm{EC}}\rangle=D/4f(x)$ is *larger* than D because $f(x)$ is a decreasing function of x. If the condition (40) is fulfilled, the one-particle Fokker-Planck equation of the kEC algorithm agrees with the ABP Fokker-Planck equation, assuring the validity of the kEC algorithm for single particles.

The strong condition $x\ll1$ can be weakened in practice because the diffusive term of the Fokker-Planck equation is only relevant for small time scales. There are three

dynamic regimes for ABPs: (i) on time scales $\Delta t < D/v_0^2$ we find translation diffusion with $\langle \Delta r^2(\Delta t)\rangle \sim D\Delta t$; (ii) on intermediate time scales $D/v_0^2 < \Delta t < \tau$ below the persistence time, the ABP performs ballistic motion with $\langle \Delta r^2(\Delta t)\rangle \sim v_0^2\Delta t^2$; (iii) on large time scales $\Delta t > \tau$, the motion becomes a persistent random walk with $\langle \Delta r^2(\Delta t)\rangle \sim v_0^2\tau\Delta t$. As a consequence, a violation of condition (40) will only give rise to a wrong translational diffusion constant that affects the short-time translational diffusion regime (i). The apparent diffusion constant $D' = D/4f(x)$ is larger than D and resulting in wrong results on time scales below the corresponding crossover time scale $\Delta t < D'/v_0^2$. As long as this erroneous behavior is limited to length scales $\langle \Delta r^2(\Delta t)\rangle < \sigma^2$, it will affect only small scale features of the distribution $P(\boldsymbol{r}, \theta, t)$ corresponding to variations below one particle diameter σ (or Fourier modes of the distribution with wave vectors $k \gtrsim 1/\sigma$). This corresponds to small time scales $\Delta t < \sigma/v_0$, and as long as $\sigma/v_0 > D'/v_0^2$, only features of the distribution below the small scale σ are wrong. This condition can be written as $3\mathrm{Pe} = v_0\sigma/D > D'/D = 1/4f(x)$ resulting in the weaker condition

$$x < 24\mathrm{Pe}/\pi \quad \text{or} \quad \ell_{\mathrm{EC}}/\sigma < 8/\pi. \tag{41}$$

In the derivation of the Fokker-Planck equation we neglected variations of the distribution $P(\boldsymbol{r}, \theta, t)$ on scales $\Delta r \lesssim \ell_{\mathrm{EC}}$, which remains consistent with neglecting variations on scales $\Delta r \lesssim \sigma$ if the condition $\ell_{\mathrm{EC}}/\sigma < 8/\pi$ holds. Under this condition, we can also neglect higher orders of the Taylor expansion in $\boldsymbol{r}$ in Eq. (34) because $\langle \Delta r^n i, \mathrm{EC}\rangle \sim \ell_{\mathrm{EC}}^n \lesssim \sigma^n$, which is also consistent with neglecting variations on scales $\Delta r < \sigma$. We conclude that we can increase $\ell_{\mathrm{EC}}/\sigma$ up to order unity if we are not interested in features of the distribution $P(\boldsymbol{r}, \theta, t)$ below one particle diameter σ.

C. Two-body problem

Regarding the two-body problem, Fig. 3 presents a section of the heatmap of the absolute value of the relative deviation per grid element $\delta_{2,\mathrm{kEC,EDBD}}$ of the two-particle probability density $p_2(\boldsymbol{r}_b, t)$ between kEC and EDBD algorithms for $\ell_{\mathrm{EC}} = 0.01\sigma$ and $\tau_B = 0.01$ from the second configuration in Fig. 4Probability density distributions $p_2(\boldsymbol{r}_b, t)$ of two hard ABPs using the EDBD algorithm (see second row, using $\tau_B = 0.01$) for two distinct initial configurations (first row) and absolute value of the relative error per grid element $\delta_{2,\mathrm{kEC,EDBD}} \equiv |(p_{2,\mathrm{kEC}} - p_{2,\mathrm{EDBD}})/p_{2,\mathrm{EDBD}}|$ of the kEC algorithm. We choose the coordinate system in a way that the position of the green particle remains fixed and measure the position of the blue particle. The results demonstrate the kEC algorithm's ability to handle interactions and collisions properly if $\ell_{\mathrm{EC}}/\sigma \to 0$figure.4 ($t = 0.05\tau$). One may notice the relative errors of the grid elements in close proximity to the coordinate-fixed particle are seemingly higher than the ones further away. Assuming the EDBD algorithm to be correct, this may suggest that the kEC algorithm is not able to handle interactions between two particles completely correctly.

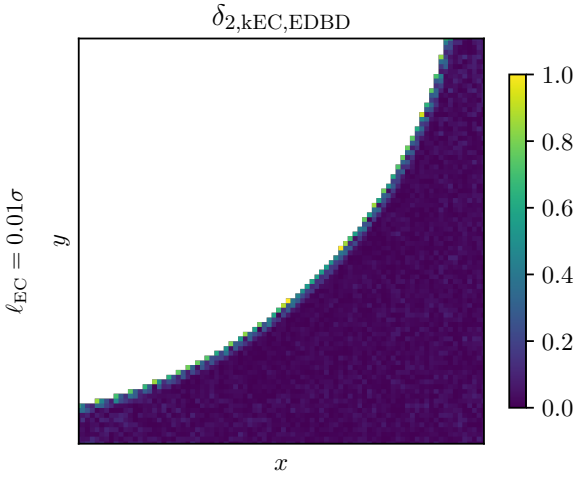

FIG. 3. A cutout section from the heatmap of the absolute value of the relative error per grid element $\delta_{2,\mathrm{kEC,EDBD}}$ of the two-particle probability density $p_2(\boldsymbol{r}, t)$ between kEC and EDBD algorithms using $\ell_{\mathrm{EC}} = 0.01\sigma$ for the second initial configuration in Fig. 4Probability density distributions $p_2(\boldsymbol{r}_b, t)$ of two hard ABPs using the EDBD algorithm (see second row, using $\tau_B = 0.01$) for two distinct initial configurations (first row) and absolute value of the relative error per grid element $\delta_{2,\mathrm{kEC,EDBD}} \equiv |(p_{2,\mathrm{kEC}} - p_{2,\mathrm{EDBD}})/p_{2,\mathrm{EDBD}}|$ of the kEC algorithm. We choose the coordinate system in a way that the position of the green particle remains fixed and measure the position of the blue particle. The results demonstrate the kEC algorithm's ability to handle interactions and collisions properly if $\ell_{\mathrm{EC}}/\sigma \to 0$figure.4 ($t = 0.05\tau$). Even though the deviations are in general relatively small, it is notable that the error per grid element seems to increase if both particles are close to each other.

This objection, or at least its relevance, can be dismissed: Similar to the role of the displacement length for the kEC algorithm, the EDBD algorithm depends on a parameter τ_B (for further information on this subject see Ref. [1]), whose choice influences the accuracy of the algorithm and is only exact in the limit of $\tau_B \to 0$. As mentioned before, we cannot prove our algorithm to be exact, but presumably decreasing both ℓ_{EC} and τ_B even further will lead to the deviations in proximity to the coordinate-fixed particle to shrink. If this is true, we can (in theory) tune both the deviations themselves as well as the length scales, on which they are relevant, at will. In practice this is of course limited to a certain degree since the required wall time increases, if the displacement length is reduced.

III. DETAILS ON THE TIME DISTRIBUTION IN MANY-BODY SIMULATIONS

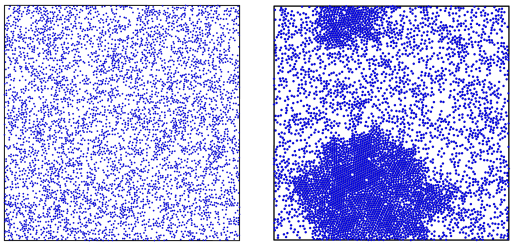

FIG. 4. Exemplary snapshots of the two systems, which were analyzed to gain insight about the behaviour of the time distribution. The system on the left with $\mathrm{Pe} = 10, \eta = 0.20, N = 5000$ is dilute and MIPS does not occcur. The system on the right with $\mathrm{Pe} = 20, \eta = 0.40, N = 5000$ is dense and exhibits MIPS. We note that system sizes are different for both system (but shown scaled to the same size), accordingly the spheres in the dense system on the right appear larger.

As previously stated every particle has its *own individual* simulation time t. This may cause problems - especially in a many-body simulation - because we would naively require that for all particles the exact same time has passed in order to maintain the correct propulsion directions (which are undergoing rotational diffusion with a persistence time τ), which is a necessary condition to also preserve the order and causality of collisions (or interactions in general). However, in statistical physics, where we are interested in statistical averages and, typically, also averages over all particles (for densities of extensive observables), this is not necessary, and it appears to be sufficient if fluctuations in time do not cause uncontrollable statistical fluctuations of observables. There are three types of averages that we have to consider in any MC or molecular dynamics simulation: (1) Statistical averages $\langle O(\Delta t)\rangle$ of a quantity $O(\Delta t)$ depending on a time difference Δt can be obtained by taking averages over many samples of the system, each after the specified time difference Δt. (2) Averages $\langle O\rangle$ of a time-independent quantity O can also be calculated as time averages over long time scales. (3) If $O = N^{-1}\sum_i O_i$ is the density of an extensive quantity, we can average over all particles, in addition to sample averaging (1) or time averaging (2). We have to check for all three types of averages how they are affected by particles having slightly different, *individual* times in the kEC simulation technique. In particular, the approach (2) to take time averages has to be applied with care.

To control the errors of any sample, time, or particle average, we have to investigate the time distribution of particles for different EC lengths, timescales, system sizes, and different phases of the system such as the dense MIPS phase or a dilute phase. We focus on two systems of $N = 5000$ particles in different parameter regimes: (i) a dilute system ($\mathrm{Pe} = 10, \eta = 0.20$), where MIPS does not occur, and (ii) a dense system ($\mathrm{Pe} = 20, \eta = 0.40$), where MIPS does occur. Exemplary snapshots can be found in Fig. 4.

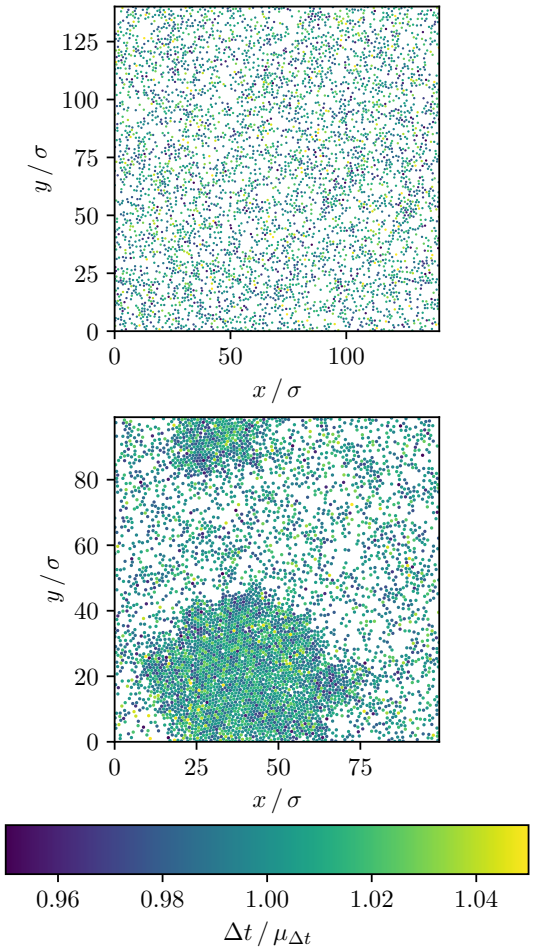

FIG. 5. Snapshot of the two systems mentioned in Fig. 4 (upper: $\mathrm{Pe} = 10, \eta = 0.20, N = 5000$, lower: $\mathrm{Pe} = 20, \eta = 0.40, N = 5000$) color-coded with respect to the individual particle times Δt at $\mu_{\Delta t} = 100\tau$ using $\ell_{\mathrm{EC}} = 1.00\sigma$. Regardless of the presence of MIPS no spatial difference in the individual particle times can be observed, implying the same time passes in each phase.

First of all, we want to investigate the distribution of passed times Δt of the particles in the dense system snapshot just mentioned. In Fig. 5 one can find the particles color-coded with respect to their individual time. It is worth noting in the case MIPS occurs one cannot find a systematic difference between the individual times of the particles in the dilute phase and the dense one. This is significant, as it proves the same time passes in the entire system regardless of the local density.

In Fig. 6, we show the distributions $p(\Delta t)$ of particle times Δt on short timescales (mean time per particle $\mu_{\Delta t} = 0.1\tau$): regardless of whether MIPS occurs the time distributions that are measured using large EC lengths are rather wide and everything but sharp. Ad-

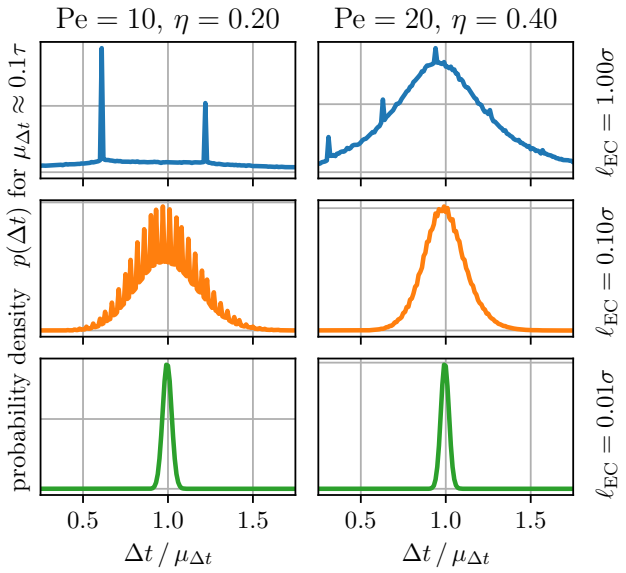

FIG. 6. Time distribution $p(\Delta t)$ depending on the EC length for the dilute system without MIPS on the left and the dense system that exhibits MIPS on the right. We focus on short timescales as the mean time passed per particle is $\mu_{\Delta t} = 0.1\tau$. For decreasing ℓ_{EC} the time distribution function $p(\Delta t)$ becomes a sharp bell-like function. Therefore the kEC algorithm can be set up in a way that for every particle almost the same time has passed.

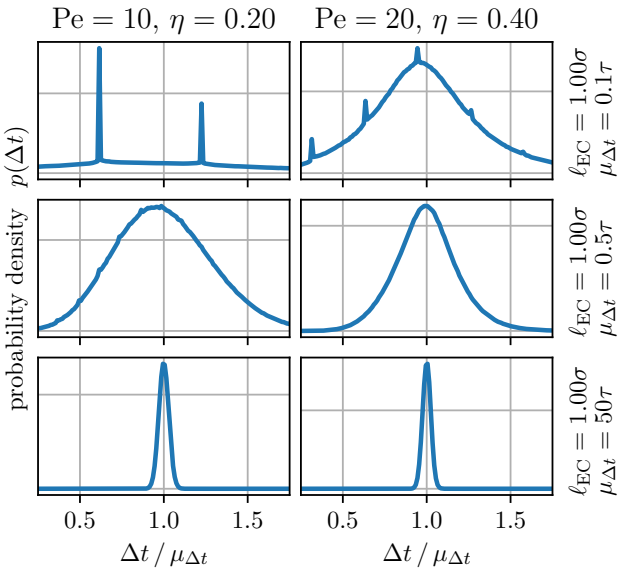

FIG. 7. Time distribution $p(\Delta t)$ for the dilute system without MIPS on the left and the dense system that exhibits MIPS on the right. We focus on medium (mean time passed per particles is $\mu_{\Delta t} = 0.5\tau$) and long ($\mu_{\Delta t} = 50\tau$) timescales. For increasing $\mu_{\Delta t}$ the time distribution function $p(\Delta t)$ becomes a bell-like function, whose relative standard deviation $c_{\Delta t} = \sigma_{\Delta t}/\mu_{\Delta t}$ steadily decreases. The apparent convergence of the relative values of the individual particle times in the limit $\mu_{\Delta t} \to \infty$ is key to satisfy the requirement that for all particles the same time must have passed.

ditionally one can observe multiple equidistant maxima, separated by the mean time per EC step $\langle \Delta t_{\mathrm{EC}} \rangle$. These maxima appear particularly in the dilute phase, if no collisions and subsequent lifting moves take place during one EC move, which results in the total time $\langle \Delta t_{\mathrm{EC}} \rangle$ being assigned to each single particle move according to Eq. (6equation.2.6). Reducing the EC length leads to an increase in the number of maxima. The reason for this is related to the non-linear relationship between $\langle \Delta t_{\mathrm{EC}} \rangle$ and the EC length. By decreasing ℓ_{EC} the mean time per EC step also gets smaller and therefore the number of EC steps per time interval increases. This implies that each particle is at least on average more often the starting point of a new EC step and due to the increase of the total displacement length more lifting moves take place. Consequently both the relative and absolute height of each peak shrinks. Because collisions (and therefore lifting moves) are in general way more frequent in a dense system, smooth shapes of the time distribution are reached for larger EC lengths as it is less probable to assign $\langle \Delta t_{\mathrm{EC}} \rangle$ to a single particle. Finally, reducing the EC length even further leads to bell-shaped time distributions, centered around the mean time per particle $\mu_{\Delta t}$, whose standard deviation $\sigma_{\Delta t}$ appears to follow a power law $\sigma_{\Delta t} \propto \ell_{\mathrm{EC}}^{\alpha}$ with an exponent $\alpha > 0$. The shape of these distributions is in some way to be expected, as we anticipate the total displacement length of each particle and therefore also the individual time to be approximately the same if the total number of EC steps and therefore the total displacement length is large.

Concerning medium ($\mu_{\Delta t} = 0.5\tau$) and long ($\mu_{\Delta t} = 50\tau$) timescales (see Fig. 7), we notice - regardless of the particle density - the relative and absolute values of the equidistant peaks separated by the mean time per EC step $\langle \Delta t_{\mathrm{EC}} \rangle$ to decrease steadily by increasing the mean time per particle $\mu_{\Delta t}$. This appears to be a rather fast process, as the maxima are barely visible already at $\mu_{\Delta t} = 0.5\tau$. Additionally and similar to reducing the EC length ℓ_{EC}, a growing mean time per particle leads to the time distribution to become bell-shaped. Furthermore the relative standard deviation $\sigma_{\Delta t}/\mu_{\Delta t}$ that corresponds to the visible width in the plots in Fig. 7, decreases as a power law $\sigma_{\Delta t}/\mu_{\Delta t} \propto \mu_{\Delta t}^{-1/2}$ as $\mu_{\Delta t}$ increases, implying the individual times of the particles are converging relatively.

Based on these observations, we investigate the relationship between the mean time per particle and the standard deviation of the time distribution and the influence of both the number of particles N as well as the EC length for the dense system Pe = 20 and $\eta = 0.40$. Fig. 8 reveals the standard deviation $\sigma_{\Delta t}$ of the time distribution to be proportional to the square root of the mean time per particle, $\sigma_{\Delta t} \propto \mu_{\Delta t}^{1/2}$. Additionally one may notice $\sigma_{\Delta t}$ to initially increase with N, reach an EC

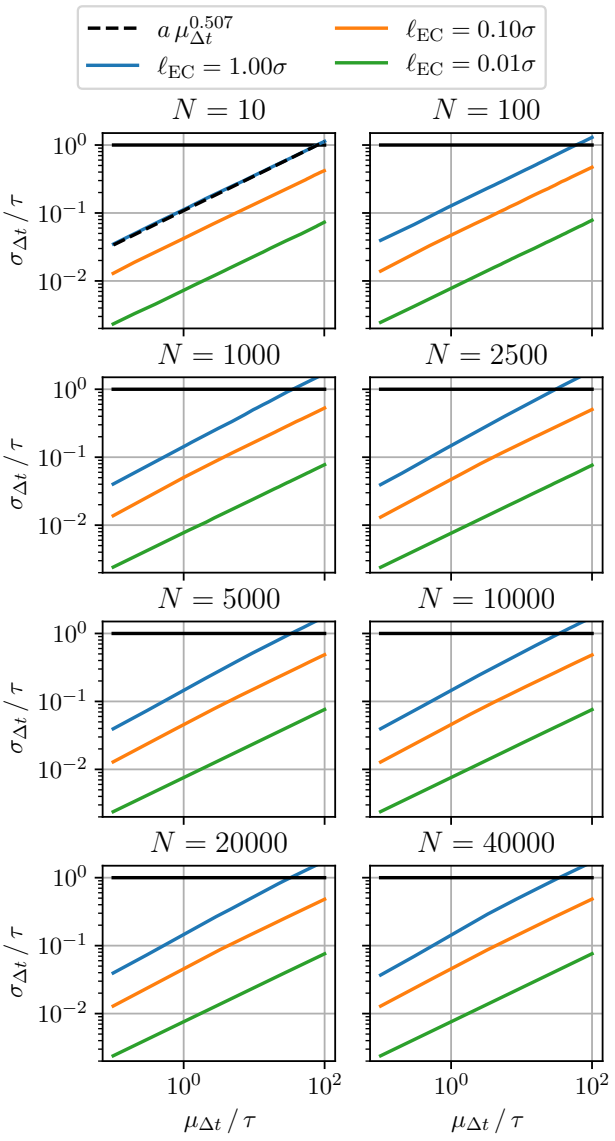

FIG. 8. Relationship between the mean time per particle and the standard deviation of the time distribution for different system sizes and displacement lengths ℓ_{EC} (Pe = 20 and $\eta = 0.40$).

length dependent peak ($N_{\mathrm{peak}} = 2500$ for $\ell_{\mathrm{EC}} = 1.00\sigma$, $N_{\mathrm{peak}} = 1000$ for $\ell_{\mathrm{EC}} = 0.10\sigma$ and $N_{\mathrm{peak}} = 100$ for $\ell_{\mathrm{EC}} = 0.01\sigma$) and afterwards to drop slightly, settle and thus become independent of N. We find

$$\sigma_{\Delta t} = a(N)\ell_{\mathrm{EC}}^{\alpha}\mu_{\Delta t}^{1/2} \tag{42}$$

with a only weakly depending on N and the exponent of ℓ_{EC} ranging from $\alpha \approx 0.46$ for $N = 10$ to $\alpha \approx 0.56$ for $N = 40000$.

As mentioned before we require the individual particle times to roughly coincide, which can be quantified by the loosely defined criterion $\sigma_{\Delta t} < \tau$, which assures that particles remain within one persistence time, i.e., the propulsion directions will not be affected by the time spread. For $\ell_{\mathrm{EC}} = 0.01\sigma$, the standard deviation satisfies $\sigma_{\Delta t} \approx 0.1\tau$ at $\mu_{\Delta t} = 100\tau$ and clearly fulfills this criterion. This implies further that we can simulate the system for several thousand persistence times using the kEC algorithm with $\ell_{\mathrm{EC}} = 0.01\sigma$ without ever violating the criterion.

The result (42) enables us to discuss the three types of statistical averages mentioned in the beginning of the section systematically: First, we notice that a width $\sigma_{\Delta t}$ of the time distribution also implies measurement errors of an observable $\Delta O(\Delta t) \sim \sigma_{\Delta t}$ after a time Δt. (1) Averages over N_s samples of a time-dependent quantity $\langle O(\Delta t)\rangle = N_s^{-1}\sum_{s=1}^{N_s} O_s(\Delta t)$ are based on the fact that the mean over N_s samples has an error $\sigma_{\langle O(\Delta t)\rangle} = N_s^{-1/2}\Delta O(\Delta t) \sim N_s^{-1/2}\sigma_{\Delta t}$, which can be controlled by the sample number as long as samples are statistically independent. The result of the additional time distribution of particles in the kEC simulation is simply that we have to average over more samples N_s for larger Δt to reduce the error of the mean. (2) Time averages over N_t times of a time-independent quantity $\langle O\rangle = N_t^{-1}\sum_{n=1}^{N_t} O(n\delta t)$ in intervals δt that should be larger than one autocorrelation time of the system have to be treated with more care because errors $\sigma_{n\delta t} \propto n^{1/2}$ grow in time according to Eq. (42). Therefore, the error $\sigma_{\langle O(\Delta t)\rangle} = (N_t^{-2}\sum_{n=1}^{N_t}\sigma_{n\delta t}^2)^{1/2} \propto N_t^0$ of such a time average is no longer reducing $\propto N_t^{-1/2}$ as usual, but actually saturating to an N_t-independent value. (3) Averages $O(\Delta t) = N^{-1}\sum_i O_i(\Delta t)$ over all particles will still be effective and reducing the error of the average $\sigma_{O(\Delta t)} \propto N^{-1/2}$ because $\Delta O(\Delta t) \sim \sigma_{\Delta t}$ is essentially N-independent according to Eq. (42).

Taking all of these information into account, our algorithm appears to be suitable to deal with many-body simulations. One can simply decrease the displacement length ℓ_{EC} to align the individual particle times, both their relative and also absolute values. This allow us to satisfy the condition $\sigma_{\Delta t} < \tau$ for very long simulation times. Typically, we only need simulation times of $20 - 50$ persistence times to reach stationary states (in case of $N = 5000$) and observe phenomena such as MIPS. Therefore we can set up the kEC algorithm in a way that for every particle (almost) the exact same time passes. This is true regardless of the presence of MIPS. Moreover, averaging over many samples or over particles are still effective ways to reduce errors of mean values. Only time averages have to be treated with care as errors of mean values saturate (with respect to the number of samples). Errors of all averages, including time averages, can be controlled by shrinking ℓ_{EC}. To avoid confusion, it should be emphasized that statistical averages - solely taking the time distribution into account - can only converge to correct values in the limit $\ell_{\mathrm{EC}} \to 0$. For large displacement lengths some of the mean values are converging, but to values related to distorted dynamics.

IV. DERIVATION OF THE N-BODY FOKKER-PLANCK EQUATION IN THE DILUTE LIMIT

In order to prove our kEC algorithm also to be exact for general N-body problem there are two problems, which one needs to overcome: (1) different individual times as a consequence of the time distribution and (2) complex algorithmic dynamics due to lifting moves. While we are currently not able to handle the second problem, one can ignore this issue in the dilute limit $\eta \to 0$. Admittedly, the system does not exhibit interesting physical phenomena such as MIPS in a pure dilute state. Nevertheless, we still want to explore this limit, because one may argue, if our algorithm is correct for the dilute N-body system it does not become discontinuously incorrect, if the packing fraction is increased to finite values.

Before dealing with the N-body Fokker-Planck equation itself, we need to make sure the exact same time passes for every particle. Let us say, we want our system to evolve for the time interval Δt ($\Delta t/\tau \ll 1$). For a given EC length, we would require m EC steps for a single particle to satisfy

$$\Delta t = m\langle \Delta t_{\mathrm{EC}} \rangle \tag{43}$$

and therefore $N \cdot m$ steps so that for each particle the time evolves on average by Δt. After $N \cdot m$ steps, the time distribution of the entire system - as demonstrated in the previous section - would be a Gaussian. We expect the standard deviation of the time distribution to shrink if one reduces the EC length, similar to the configuration we discussed in Sec. III. In other words: $\ell_{\mathrm{EC}} \to 0$ automatically leads to $\sigma_{\Delta t} \to 0$. However, a Gaussian distribution with vanishing standard deviation is a δ-distribution

$$\lim_{\sigma_{\Delta t}\to 0} \mathrm{Gaussian}(\mu_{\Delta t}, \sigma_{\Delta t}) = \delta(t - \mu_{\Delta t}). \tag{44}$$

This way, we can make sure that all individual particle times are exactly the same.

Let $P(\boldsymbol{r}_1, ..., \boldsymbol{r}_N, \theta_1, ..., \theta_N, t_1, ..., t_N)$ be the probability density of the dilute (non-interacting) N-body system. In the limit $\ell_{\mathrm{EC}} \to 0$ all individual times are the same and $t_i = t$ holds. To find the N-body Fokker-Planck equation we need to find an expression for $P(\{\boldsymbol{r}_i\}, \{\theta_i\}, t + \Delta t) \equiv P(\boldsymbol{r}_1, ..., \boldsymbol{r}_N, \theta_1, ..., \theta_N, t + \Delta t)$. In Sec. II B we found

$$\begin{aligned} &P(\boldsymbol{r}, \theta, t + \langle \Delta t_{\mathrm{EC}} \rangle) \\ &\approx P(\boldsymbol{r}, \theta, t) - v_0 \langle \Delta t_{\mathrm{EC}} \rangle \boldsymbol{e}(\theta) \boldsymbol{\nabla}_{\boldsymbol{r}} P(\boldsymbol{r}, \theta, t) \\ &+ D_r \langle \Delta t_{\mathrm{EC}} \rangle \partial_\theta^2 P(\boldsymbol{r}, \theta, t) + D \langle \Delta t_{\mathrm{EC}} \rangle \boldsymbol{\nabla}_{\boldsymbol{r}}^2 P(\boldsymbol{r}, \theta, t). \end{aligned} \tag{45}$$

We can use this formula iteratively and ignore all terms smaller than $\mathcal{O}(\langle \Delta t_{\mathrm{EC}} \rangle)$, which leads to

$$\begin{aligned} &P(\boldsymbol{r}, \theta, t + m\langle \Delta t_{\mathrm{EC}} \rangle) \\ &\approx P(\boldsymbol{r}, \theta, t) - v_0 m \langle \Delta t_{\mathrm{EC}} \rangle \boldsymbol{e}(\theta) \boldsymbol{\nabla}_{\boldsymbol{r}} P(\boldsymbol{r}, \theta, t) \\ &+ D_r m \langle \Delta t_{\mathrm{EC}} \rangle \partial_\theta^2 P(\boldsymbol{r}, \theta, t) + D m \langle \Delta t_{\mathrm{EC}} \rangle \boldsymbol{\nabla}_{\boldsymbol{r}}^2 P(\boldsymbol{r}, \theta, t). \end{aligned} \tag{46}$$

In the dilute (non-interacting) limit all coordinates are completely independent of each other. This allows us to employ the same procedure, we just used for a single ABP, to obtain

$$\begin{aligned} &P(\{\boldsymbol{r}_i\}, \{\theta_i\}, t + \Delta t) = P(\{\boldsymbol{r}_i\}, \{\theta_i\}, t + m\langle t_{\mathrm{EC}} \rangle) \\ &\approx P(\{\boldsymbol{r}_i\}, \{\theta_i\}, t) \\ &+ m\langle t_{\mathrm{EC}} \rangle \sum_{i=1}^{N} \Big(- v_{0,i} \boldsymbol{e}_i \boldsymbol{\nabla}_{\boldsymbol{r}_i} + D_r \partial_{\theta_i}^2 + D \boldsymbol{\nabla}_{\boldsymbol{r}_i}^2 \Big) \\ &\quad P(\{\boldsymbol{r}_i\}, \{\theta_i\}, t). \end{aligned} \tag{47}$$

This can easily be transformed to

$$\begin{aligned} &\partial_t P(\{\boldsymbol{r}_i\}, \{\theta_i\}, t) \\ &\approx \sum_{i=1}^{N} \Big(- v_{0,i} \boldsymbol{e}_i \boldsymbol{\nabla}_{\boldsymbol{r}_i} + D_r \partial_{\theta_i}^2 + D \boldsymbol{\nabla}_{\boldsymbol{r}_i}^2 \Big) P(\{\boldsymbol{r}_i\}, \{\theta_i\}, t), \end{aligned} \tag{48}$$

which we identify as the correct N-body Fokker-Planck equation of non-interacting ABPs.

V. DETAILS OF THE KEC SIMULATIONS FOR THE PHASE DIAGRAM OF HARD DISKS

To construct the large phase diagram in Fig. 6Left: Phase diagram of active hard disks (kEC: $N = 19500$ and area A changing according to the packing fraction η) from kEC simulations using $\ell_{\mathrm{EC}} = 1.00\sigma$. The kEC results for the binodal in general agree with EDBD simulation results ($N = 2000 - 4000$) of Levis *et al.* [1] except for some deviations around the critical point. Right: Phase diagram of active hard disks (kEC: $N = 5000$) using different values for the EC length. In agreement with the previous observations, reducing ℓ_{EC} leads to better results, especially around the critical point. The remaining deviations are most likely an artifact of different system sizes and ways of calculating the binodalfigure.6 in the main text, we simulate $N = 19500$ particles using $\ell_{\mathrm{EC}} = 1.00\sigma$ in a square box with area $A = L^2$ and periodic boundary conditions. We change the global packing fraction $\eta = N\pi(\sigma/2)^2/A$ by changing the system size L at a fixed particle number. Depending on the Péclet number $\mathrm{Pe} = v_0/(\sigma D_r) = L_p/\sigma$ and the global packing density, the phase behavior is classified and the binodal is determined.

A. Calculating the distribution of the local packing fraction

The investigation of the MIPS phase and its stability is performed via calculating the probability density distribution $p(\eta_{\mathrm{local}})$ of the local packing fraction, see Fig. 9. In order to calculate this quantity, we first divide the simulation volume into multiple subvolumes, each of which

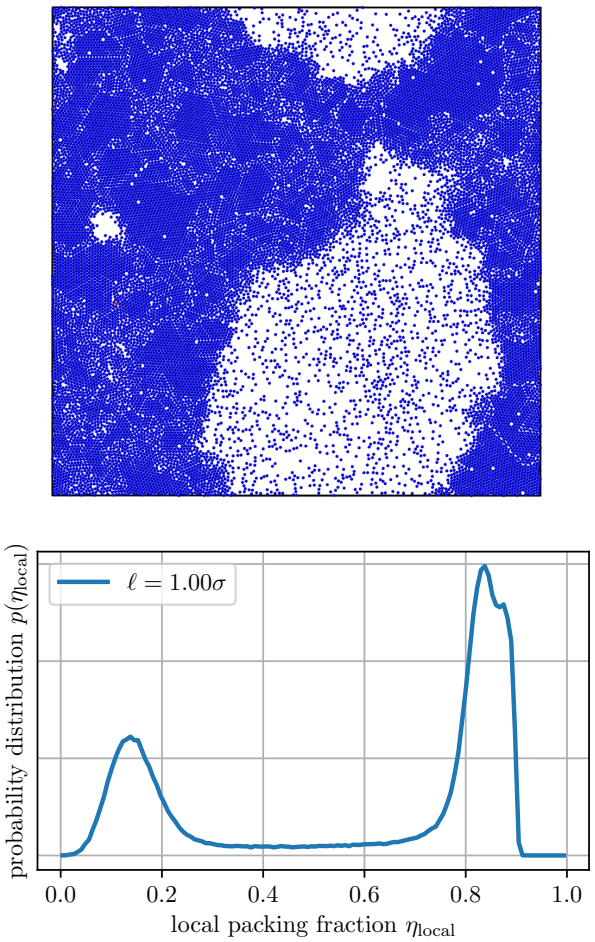

FIG. 9. (a) Snapshot of a system exhibiting MIPS at Pe = 30 and $\eta = 0.60$ ($N = 19500$, $\ell_{\text{EC}} = 1.00\sigma$). (b) Corresponding histogram of local packing fractions η_{local} using cells of area $A_h \approx (7\sigma)^2$.

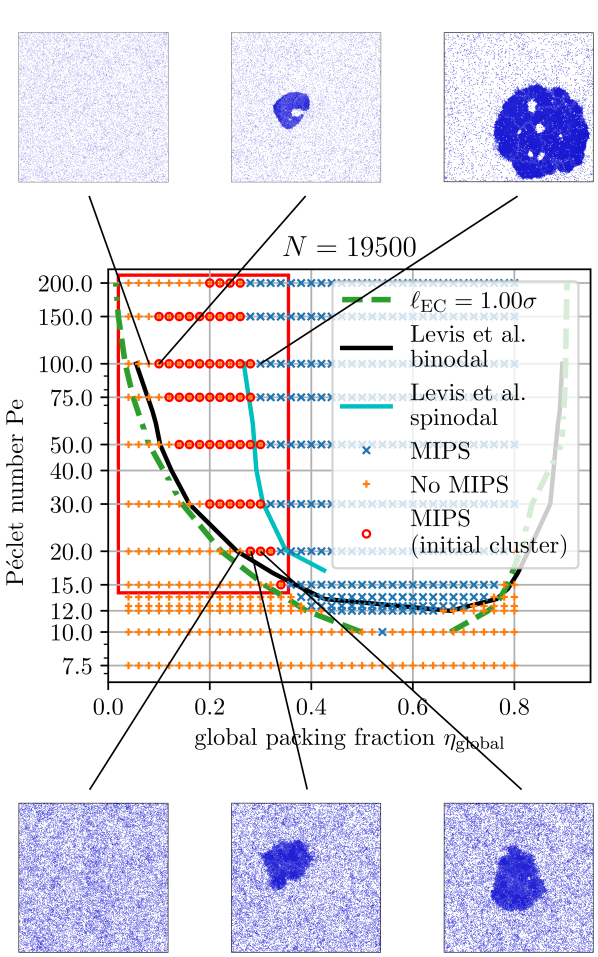

FIG. 10. Results of additional simulations with phase-separated initial state in the phase region enclosed by the red rectangle. The red circles are simulations with final states that show MIPS as indicated for some examples in the insets. This confirms that the boundary between blue and orange points represents a spinodal line.

has the area $A_h \approx (7\sigma)^2$. We calculate the local density in each of those subvolumes and (by averaging over many snapshots) use this data to construct the probability density distribution $p(\eta_{\text{local}})$ of the local packing fraction.

B. Determination of binodal and spinodal lines

To determine the binodal line, we calculate the probability density distribution $p(\eta_{\text{local}})$ of the local packing fraction. If MIPS occurs, $p(\eta_{\text{local}})$ exhibits two distinct maxima corresponding to the dilute and dense phase (see Fig. 9). The binodal lines indicate the coexisting densities and are determined by averaging the coexisting densities (the positions of the two maxima of $p(\eta_{\text{local}})$) for different global packing fractions at the same Péclet number.

Orange points in Fig. 6Left: Phase diagram of active hard disks (kEC: $N = 19500$ and area A changing according to the packing fraction η) from kEC simulations using $\ell_{\text{EC}} = 1.00\sigma$. The kEC results for the binodal in general agree with EDBD simulation results ($N = 2000 - 4000$) of Levis *et al.* [1] except for some deviations around the critical point. Right: Phase diagram of active hard disks (kEC: $N = 5000$) using different values for the EC length. In agreement with the previous observations, reducing ℓ_{EC} leads to better results, especially around the critical point. The remaining deviations are most likely an artifact of different system sizes and ways of calculating the binodalfigure.6 of the main text, which lie within the region spanned by the binodal line, correspond to global packing fractions, where the homogeneous initial state is only metastable. They should become unstable to MIPS by strong perturbations, such as strong density

fluctuations. To check this, some systems are simulated with $\eta \leq 0.32$, similar to Ref. [1], with an already phase-separated initial state, which we prepared by placing a dense and approximately square-shaped particle cluster in the center of the system. In addition, all initial driving forces are aligned in the direction of the system center. The results are shown in Fig. 10, where red circles represent systems with phase-separated final states (see insets). We find that the phase-separated state is globally stable, while the homogeneous state is only metastable, for most of the orange points, which lie between the coexistence lines. Small deviations, especially near the binodal, are due to finite-size effects cf. to a free energy barrier of homogeneous nucleation.

The method to calculate the binodal lines, which was previously explained, does not work close to the critical point. This is because in proximity of $(\eta_{\mathrm{crit}}, \mathrm{Pe}_{\mathrm{crit}})$ one cannot determine the peaks related to the dilute and dense phase, as they are barely set apart from the rest of the distribution and become virtually indistinguishable from small fluctuations of $p(\eta_{\mathrm{local}})$. Of course one can deal with these problems by increasing the sample and system size, which would lead to an increase of the overall computational effort.

VI. HANDLING OF NON-PERIODIC BOUNDARY CONDITIONS AND EXTERNAL POTENTIALS

Throughout this work we have focused on periodic boundary conditions, however certain problems require non-periodicity via soft or hard walls. Since soft walls can be viewed as short-ranged external potentials and hard walls are the infinitely steep limit of the former, we will briefly address how to incorporate external one-particle potentials into our algorithm.

Before dealing with the kEC algorithm, we should take a closer look at the dynamics of the new setup. In the presence of an external potential the equation of motion for an isolated particle takes the form

$$\dot{\boldsymbol{r}}(t) = v_0 \boldsymbol{e}(t) + \boldsymbol{\xi}(t) - \frac{1}{\Gamma} \boldsymbol{F}_{\mathrm{ext}}(\boldsymbol{r}), \tag{49}$$

which leads - in the limit of small timesteps - to the mean displacement

$$\begin{aligned} \langle \Delta \boldsymbol{r} \rangle &\approx \Big(v_0 \boldsymbol{e} - \frac{1}{\Gamma} \boldsymbol{F}_{\mathrm{ext}}(\boldsymbol{r}) \Big) \Delta t \\ &= \Big(v_0 \boldsymbol{e} - v_{\mathrm{ext}} \boldsymbol{e}_{\mathrm{ext}} \Big) \Delta t. \end{aligned} \tag{50}$$

As mentioned in the beginning, a rejection caused by an external potential leads to a reflection of the displacement direction at the potentials equipotential surface. There are two possibilities of adjusting the mean time per EC move for an active particle: One could either calculate the mean move vector $\langle \Delta \boldsymbol{r}_{\mathrm{EC}} \rangle$ during one ECMC step for an algorithm that handles the active force and external potential separately, or we consider an algorithm that combines both active and external force into one potential. The first option keeps up the idea that each interaction can be handled entirely independently in the ECMC algorithm through factorization of the Metropolis filter, but it is also way more complicated to calculate $\langle \Delta \boldsymbol{r}_{\mathrm{EC}} \rangle$ for such a factorized version of the algorithm. Therefore, we strongly suggest to use the second option. As the previous analysis proved, the dynamics of a single free ABP is correct in the limit $\ell_{\mathrm{EC}}/\sigma \to 0$. As we expect the same to be true in the presence of an external potential, we can approximate any potential during a single EC step as a linear potential (this is the same idea as the assumption of small timesteps in Eq. (50)). This allows us to calculate $\langle \boldsymbol{r}_{\mathrm{EC}} \rangle$ analogously to Sec. I B using the combined total force $F_{\mathrm{tot}} = |F_0 \boldsymbol{e} - F_{\mathrm{ext}} \boldsymbol{e}_{\mathrm{ext}}|$ instead of F_0 and $\boldsymbol{e}_{\mathrm{tot}} = \boldsymbol{F}_{\mathrm{tot}}/F_{\mathrm{tot}}$ instead of $\boldsymbol{e}$. In case of short-ranged potentials and/or nonlinear potentials this procedure causes the mean time per EC step to depend on the position of the particle $\langle \Delta t_{\mathrm{EC}}(\boldsymbol{r}) \rangle$. This may raise the concern, that the individual particle times may vary greatly. However, because of the shape of the time function $f(x)$ we expect the particle times to coincide at least in the limit $x \to 0$ and therefore the limit of vanishing EC lengths.

[1] D. Levis, J. Codina, and I. Pagonabarraga, Active Brownian equation of state: Metastability and phase coexistence, Soft Matter **13**, 8113 (2017).